Specific and Efficient Binding of Xeroderma Pigmentosum Complementation Group A to Double-Strand/Single-Strand DNA Junctions with 3′- and/or 5′-ssDNA Branches†

Zhengguan Yang,‡ Marina Roginskaya,‡ Laureen C. Colis,§ Ashis K. Basu,§ Steven M. Shell,‡ Yiyong Liu,‡ Phillip R. Musich,‡ Constance M. Harris,|| Thomas M. Harris,|| and Yue Zou*,‡

Department of Biochemistry and Molecular Biology, James H. Quillen College of Medicine, East Tennessee State University, Johnson City, Tennessee 37614, Department of Chemistry, University of Connecticut, Storrs, Connecticut 06269, and Chemistry Department and Center in Molecular Toxicology, Vanderbilt University, Nashville, Tennessee 37235

Received August 10, 2006; Revised Manuscript Received October 25, 2006

ABSTRACT: Human XPA is an important DNA damage recognition protein in nucleotide excision repair (NER). We previously observed that XPA binds to the DNA lesion as a homodimer [Liu, Y., Liu, Y., Yang, Z., Utzat, C., Wang, G., Basu, A. K., and Zou, Y. (2005) *Biochemistry 44*, 7361−7368]. Herein we report that XPA recognized undamaged DNA double-strand/single-strand (ds-ssDNA) junctions containing ssDNA branches with binding affinity ($K_d = 49.1 \pm 5.1$ nM) much higher than its ability to bind to DNA damage. The recognized DNA junction structures include the Y-shape junction (with both 3′- and 5′-ssDNA branches), 3′-overhang junction (with a 3′-ssDNA branch), and 5′-overhang junction (with a 5′-ssDNA branch). Using gel filtration chromatography and gel mobility shift assays, we showed that the highly efficient binding appeared to be carried out by the XPA monomer and that the binding was largely independent of RPA. Furthermore, XPA efficiently bound to six-nucleotide mismatched DNA bubble substrates with or without DNA adducts including C8 guanine adducts of AF, AAF, and AP and the T[6,4]T photoproducts. Using a set of defined DNA substrates with varying degrees of DNA bending, we also found that the XPC−HR23B complex recognized DNA bending, whereas neither XPA nor the XPA−RPA complex could bind to bent DNA. We propose that, besides DNA damage recognition, XPA may also play a novel role in stabilizing, via its high affinity to ds-ssDNA junctions, the DNA strand opening surrounding the lesion for stable formation of preincision NER intermediates. Our results provide a plausible mechanistic interpretation for the indispensable requirement of XPA for both global genome and transcription-coupled repairs. Since ds-ssDNA junctions are common intermediates in many DNA metabolic pathways, the additional potential role of XPA in cellular processes is discussed.

Nucleotide excision repair (NER)[1] is an important DNA repair pathway that removes a broad variety of bulky or distorting DNA damages induced by chemicals and UV light (*2*−*4*). XPA (xeroderma pigmentosum group A) is an indispensable factor for both global genome repair (GGR) and transcription-coupled repair (TCR), the two subpathways of NER (*2*−*5*). It is believed that XPA is involved in the DNA damage recognition in NER (*1*, *2*, *4*). XPA−DNA damage interaction is carried out in a cooperative manner by the XPA dimer (*1*, *6*). Other DNA damage recognition proteins in NER include RPA (replication protein A) and the XPC−HR23B complex. The latter is believed to be the initial damage recognition factor, though it is required only for GGR (*7*). In TCR, where the XPC−HR23B is not required, the RNA polymerase complex may play a role for initial damage recognition, while the role of XPA remains unclear. XPA is believed to form a complex with RPA to stabilize or mediate the RPA−DNA interaction (*8*−*10*). However, recent studies indicate that XPA may be loaded as a separate factor to DNA lesions in cells (*11*, *12*) and the presence of XPA or RPA has little effect on damaged DNA binding affinity of either protein (*1*, *13*). Furthermore, XPA acts as a co-recognition factor with the XPC−HR23B complex in recognizing triplex-directed psoralen DNA interstrand cross-links (*14*). A crucial role of XPA in NER was demonstrated by its involvement in both GGR and TCR, its presence in damage recognition through preincision complex assembling, and its being a limiting factor for NER and UV sensitivity in human cells (*15*).

Although the functions of XPA have been extensively studied, its exact role in NER remains elusive. Recent studies

† This study was supported by NCI Grant CA86927 (to Y.Z.) and NIEHS Grants ES09127 and ES013324 (to A.K.B.).

* Corresponding author. Phone: (423) 439-2124. Fax: (423) 439-2030. E-mail: zouy@etsu.edu.

‡ East Tennessee State University.

§ University of Connecticut.

|| Vanderbilt University.

[1] Abbreviations: NER, nucleotide excision repair; XPA, xeroderma pigmentosum complementation group A; RPA, replication protein A; XPC, xeroderma pigmentosum complementation group C; IPTG, isopropyl β-D-thiogalactoside; DTT, dithiothreitol; EDTA, ethylenediaminetetraacetic acid; AF, 2-aminofluorene; AAF, *N*-acetyl-2-aminofluorene; AP, 1-amionopyrene; GT, G[8,5-ME]T tandem lesion; T[6,4]T, TT cross-link 6,4-photoproducts; BD, bending DNA substrates; GGR, global genome repair; TCR, transcription-coupled repair; ds-ssDNA, double-strand/single-strand junctions of DNA.

10.1021/bi061626q CCC: $33.50
Published on Web 12/19/2006

have showed that XPA efficiently binds to double-stranded three-way or four-way (Holliday junction-type) DNA structures (*16*), which appears to be correlated with repair efficiency (*17*). However, these structures are absent in NER intermediates, although the results have been suggested to support XPA recognition of the helical kinks induced by DNA damage (*17*). Besides its role in DNA damage recognition, XPA also has been suggested to be important for recruitment of other NER factors for nuclease assembly for incisions (*4*, *18*−*21*). The recruitment of Rad1−Rad10, the yeast homologue of XPF−ERCC1, by Rad14, the yeast homologue of XPA (*22*), has recently been demonstrated in vivo, even though the mechanism for this process remains unclear. Also importantly, several recent sudies suggested that XPA may play additional roles in cellular DNA damage responses via its phosphorylation and possible involvement in DNA damage checkpoints (*39*, *42*, *43*).

In the present study we report a potential novel function of XPA in NER. Using a homogeneous form of XPA purified from baculovirus-infected insect cells (*1*), we demonstrated that, in addition to efficient interaction with damaged DNA substrates containing C8 guanine adducts of AF, AAF, or AP and the G[8,5-Me]T vicinal cross-link, XPA has an unusually high affinity for ds-ssDNA junctions with 3′- and/or 5′-ssDNA overhangs (including Y-structure junction and the junctions with either a 3′- or 5′-ssDNA branch). This DNA junction binding was carried out by the XPA monomer, whereas the DNA damage recognition is performed by the XPA dimer. Also noteworthy is the finding that XPA exhibited no significant difference in its affinity for different types of DNA adducts when contained in a six-nucleotide bubble structure. Furthermore, using a set of structure-specific DNA substrates with various degrees of bending angle, we showed that XPA had almost no affinity and specificity for bent DNA. By contrast, the XPC−HR23B complex could bind efficiently and with high specificity to the bent DNA substrates. Our data support a novel role for XPA in NER to stabilize the unwound DNA intermediate surrounding the lesion, which may also facilitate the recruitment of NRE factors for nuclease assembly.

MATERIALS AND METHODS

Chemicals and Reagents. All chemicals, including Tris·HCl, Hepes, NaCl, $ZnCl_2$, $CaCl_2$, $MgCl_2$, boric acid, EDTA, glycerol, ammonium persulfate, phenylmethanesulfonyl fluoride (PMSF), *N*,*N*,*N*′,*N*′-tetramethylethylenediamine (TEMED), β-mercaptoethanol, and imidazole were purchased from Fisher Scientific Co. or Sigma Co. Ni-NTA beads were purchased from Qiagen. Chitin beads were purchased from New England Biolabs. Polyacrylamides and urea were obtained from Bio-Rad and National Diagnostics. Protease inhibitor cocktail was obtained from Roche Co. XPA antibody was obtained from Kamiya Biotech Inc., and anti-RPA 70, 32, and 14 antibodies were obtained from Santa Cruz Biotechnology Inc.

XPA and RPA Protein Purification. $[His]_6$-XPA protein was purified from Sf21 insect cells infected with recombinant baculovirus pBac-XPA virus (graciously provided by J. J. Turchi, Wright State University School of Medicine) at a multiplicity of infection (moi) of 10 as described previously (*1*). RPA protein was expressed in BL21(DE3)-RP competent cells (Stratagene) and induced with 0.7 mM IPTG at 25 °C for 3 h. Recombinant RPA was purified using chitin affinity beads in a one-step procedure as described previously (*6*, *23*). Briefly, chitin-bound RPA was eluted in 30 mM DTT cleavage buffer, and RPA-positive fractions were pooled and concentrated. The eluted fractions containing RPA trimer were collected and dialyzed in RPA storage buffer containing 50% glycerol. XPA and RPA protein concentrations were determined using the Bio-Rad protein assay following the manufacturer's instructions.

XPC−HR23B Protein Complex Purification. The XPC−HR23B protein complex was purified as described previously (*24*). XPC−HR23B protein was purified from Sf21 insect cells infected with recombinant baculovirus expressing XPC and HR23B proteins (graciously provided by A. Sancar, University of North Carolina, Chapel Hill). Briefly, 500 mL of Sf21 cells was infected with recombinant pBacXPC-HR23B baculovirus at a multiplicity of infection of about 10 and incubated at 27 °C for 48 h. Cells were harvested by low-speed (2000 rpm) centrifugation, and cell free extracts were prepared (*25*, *26*). Cell pellets were resuspended in 20 mL of lysis buffer [10 mM Tris·HCl, pH 7.9, 1 mM EDTA, 5 mM dithiothreitol (DTT), and 0.5 mM PMSF plus 1× Roche protease inhibitor cocktail], incubated on ice for 20 min, and homogenized using a Dounce homogenizer by eight strokes with a "B" pestle. To this suspension were added 20 mL of buffer [50 M Tris·HCl, pH 7.9, 10 mM $MgCl_2$, 2 mM DTT, and 50% glycerol (v/v)] and sucrose, followed by gentle stirring until sucrose completely dissolved in the buffer (final concentration of sucrose is 12.5%). Subsequently, 6 mL of saturated $(NH_4)_2SO_4$ was added drop by drop with gentle stirring over 20 min. The extracts were clarified by centrifugation for 3 h at 50000 rpm in a Beckman ultracentrifuge using a 50 Ti rotor at 4 °C. The resulting supernatant was dialyzed against buffer A (25 mM Tris·HCl, pH 7.5, 1 mM EDTA, 1 mM DTT, 0.01% Triton X-100, and 10% glycerol) containing 0.3 M KCl for 2 h. Dialyzed extracts were further centrifuged for 10 min at 12000*g* at 4 °C, and the supernatant was loaded onto a 12 mL cellulose phosphate column (Whatman) equilibrated in the same buffer. The column was washed with 100 mL of buffer A (plus 0.3 M KCl) and eluted with 50 mL of buffer A (plus 1 M KCl). Eluted protein was pooled and diluted to 0.6 M KCl with buffer A without KCl. Diluted protein was applied to a 5 mL ssDNA cellulose column (Sigma) equilibrated with buffer A (0.6 M KCl), and the column was washed with 100 mL of buffer A (0.6 M KCl). Eluted protein was diluted with buffer A to 0.3 M KCl and applied to a 1 mL HiTrap DEAE FF column (Amersham Biosciences). Flow-through fractions containing XPC−HR23B were collected and dialyzed against storage buffer and stored at −80 °C in aliquots. Protein concentration was determined using the Bio-Rad protein assay. The purity of the XPC−HR23B complex was confirmed by SDS−PAGE (10%) and Western blotting.

Substrate Construction. Substrates were constructed as described previously (*27*, *28*). Briefly, 50 bp substrates were constructed by annealing equimolar amounts of either damaged or undamaged 10-mer or 11-mer with flanking 19-mer and 5′-^{32}P-radiolabeled 20-mer in the presence of a complementary 44-mer (bottom strand), followed by ligation with 0.5 unit of T4 DNA ligase overnight at 16 °C. The ligation products were purified on a 12% denaturing gel,

reannealed with a complementary 50-mer (bottom strand), which was again purified on an 8% native gel. Fifty base pair bubble substrates were constructed using the same protocol with the following modifications: the purified ligated 50-mer containing a DNA lesion (top strand) was reannealed with a partially complementary 50-mer containing the indicated number of mismatched nucleotides. The 49 bp T[6,4]T and G[8,5-Me]T intrastrand cross-link substrates were constructed as reported (*29*). The substrates containing a G[nc]G intrastrand cross-link were synthesized and constructed as described previously (*30*). The G[nc]G lesion is the guanine−guanine binucleotides cross-linked with a two-, three-, or four-carbon tether. The n in the G[nc]G stands for the number of carbons in the tether, while the c stands for carbon.

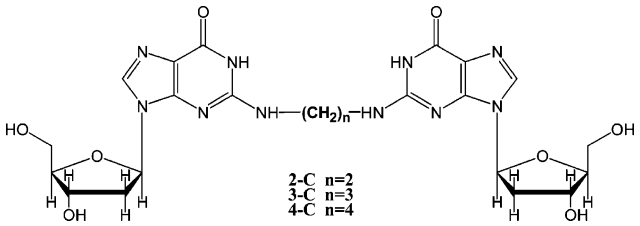

The ds-ssDNA junction substrates with ssDNA overhangs were constructed by annealing the 5′-terminally ^{32}P-radiolabeled top strand with different bottom strands, followed by purification on an 8% native gel. All substrates were subjected to restriction enzyme analysis with *Hae*III and/or *Ras*I to verify proper alignment of the final products.

Electrophoretic Mobility Shift Assay (EMSA). Binding of XPA, RPA, XPA−RPA, and XPC−HR23B to various DNA substrates was analyzed by gel mobility shift assay as described previously (*1*, *6*). Typically, substrates (0.5−1 nM) were incubated with varying concentrations of protein at 30 °C in 20 μL of binding buffer [20 mM Hepes−KOH, pH 7.9, 75 mM KCl, 5 mM $MgCl_2$, 1 mM DTT, 5% glycerol, 100 μg/mL acetylated BSA (Promega)]. Reactions were then placed on ice, 2 μL of 80% (v/v) glycerol was added, and the mixture was immediately loaded onto a 3.5% native polyacrylamide gel and electrophoresed at 80 V in 1× TBE buffer for 2 h at 4 °C. The gels were dried and exposed to phosphoimage screens overnight. Quantification of the radioactivity was carried out using a Fuji FLA-5000 scanner with the ImageGuage software.

Fluorescence Anisotropy Analysis. Anisotropy titrations were performed as described previously (*23*) to characterize the XPA binding to the ds-ssDNA junction (5′-terminally labeled with a fluorescein on the top strand) in the buffer containing 20 mM Hepes-KOH, pH 7.9, 75 mM KCl, 5 mM $MgCl_2$, 2 mM DTT, 5% glycerol, and 200 μg/mL human serum albumin (a gracious gift from Dr. David Johnson, East Tennessee State University). The data were analyzed using a one-site binding model and the nonlinear least-squares method for the determination of the dissociation constants (*1*, *31*).

DNase I and Permanganate Footprinting Assays. The DNase I footprinting assay was carried out as described previously (*32*). Prior to DNase I digestion, 3′-terminally labeled Y-shape substrates (8 nM) were incubated in the presence and absence of 200 nM XPA (an equal amount of XPA storage buffer was added for no XPA conditions) at 30 °C for 15 min in 10 μL of binding buffer [20 mM Hepes−KOH, pH 7.9, 75 mM KCl, 5 mM $MgCl_2$, 1 mM EDTA, 1 mM DTT, 5% glycerol, and 100 μg/mL BSA (Promega)]. After incubation, $CaCl_2$ was added to 10 mM final concentration. Substrates were then digested with 0.7 ng of DNase I (Invitrogen) at room temperature for 1 min. The reactions were terminated by adding 10 μL of formamide DNA-denaturing buffer containing 40 mM EDTA, and the samples were immediately frozen in the dry ice−ethanol mixture. The samples were heated to 90 °C for 5 min, immediately chilled on ice, and subjected to electrophoresis in 12% polyacrylamide sequencing gel (8 M urea) under denaturing conditions.

The chemical footprinting assay was conducted according to procedures described previously (*33*). Briefly, labeled Y-shape substrates (8 nM) were incubated in 10 μL of binding buffer with 200 nM XPA or without XPA as described in the previous section. Then 2.5 μL of $KMnO_4$ was added (0.2 mM final concentration), and the reactions were conducted at room temperature for 1 min. Reactions were terminated by adding an equal volume of 2 M 2-mercapthoethanol containing 40 mM EDTA, immediately followed by chilling on ice. The DNA was precipitated with 70% cold ethanol and then incubated with 25 μL of 1 M piperidine at 90 °C for 25 min. Samples were spin-vacuumed and analyzed on a 12% sequencing gel under denaturing conditions.

Size Exclusion Chromatography/Liquid Scintillation Assay. Gel filtration chromatography coupled with scintillation analysis was employed to analyze the stoichiometry of XPA binding to the ds-ssDNA junction substrate. Briefly, the substrate (1 nM) was incubated with varying concentrations of protein at 30 °C in 100 μL of binding buffer for 30 min. After incubation, the reactions were loaded onto a Superdex 200 size exclusion column (Amersham Pharmacia Biosciences, Uppsala, Sweden) and eluted with XPA binding buffer (20 mM Hepes−KOH, pH 7.9, 75 mM KCl, 5 mM $MgCl_2$, 1 mM DTT, and 5% glycerol). Fractions of 0.2−0.5 mL were collected using a Frac-900 autocollector (Amersham Pharmacia Biosciences, Uppsala, Sweden). One hundred microliters of each fraction was mixed with 5 mL of ScintiSafe 30 scintillation cocktail (Fisher Scientific Inc.), and radioactivity was counted using a Beckman LS 3801 liquid scintillation system. Under the same conditions, 100 μL of standard protein markers also was loaded onto Superdex 200 size exclusion column and eluted by the same buffer. The standard protein markers included ribonuclease A (13.7 kDa), chymotrypsinogen A (25 kDa), ovalbumin (43 kDa), bovine albumin (67 kDa), aldolase (158 kDa), catalase (232 kDa), ferritin (440 kDa), and thyroglobulin (669 kDa). A linear relationship between the protein molecular weights (log MW) and retention volume (mL) was established by linear regression.

RESULTS

Protein Purification. Recombinant XPA and XPC−HR23B proteins overexpressed in baculovirus-infected insect cells were purified following the procedures as described in Materials and Methods. Purified XPA exhibited homogeneity as analyzed on 10% SDS−PAGE (*1*). RPA was purified from *Escherichia coli* BL21(DE3)-RP cells transformed with the overexpressing plasmid pTYB-RPA containing RPA cDNA

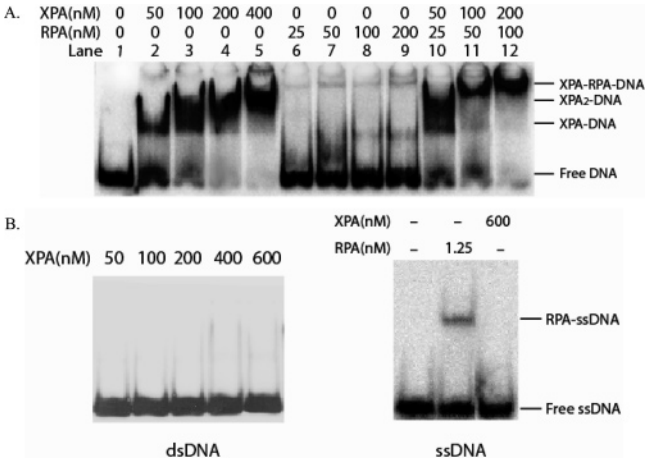

FIGURE 1: XPA binding to the DNA duplex containing a G[8,5-Me]T cross-link lesion. Panel A: Homogeneous XPA protein purified from baculovirus-infected insect cells showed high specific affinity to the 50 bp DNA substrate containing a γ-radiation-induced G[8,5-Me]T cross-link lesion in the presence and absence of RPA in gel mobility shift assays. RPA protein itself displayed no affinity for the DNA cross-link adduct (lanes 6−9), although the presence of RPA resulted in a supershift of XPA−DNA bands corresponding to the XPA−RPA−DNA interaction (lanes 10−12). Panel B: XPA protein showed little or no affinity for the undamaged DNA duplex or ssDNA. Gel mobility shift assays were performed on 3.5% native polyacrylamide gel electrophoresed at 4 °C.

(*6*, *23*). All of these proteins have purity greater than 95% (data not shown). The XPA and XPC−HR23B proteins were fully active to recognize damaged DNA substrates with various adducts (see below). Purified RPA also had full activity toward single-stranded DNA (data not shown).

Binding of XPA to a DNA Substrate Containing a G[8,5-Me]T Cross-Link Lesion. Electrophoretic mobility shift assay (EMSA) was used to examine the affinity and specificity of the XPA protein for damaged versus undamaged DNA. As shown in Figure 1, XPA had a high specific affinity for damaged DNA substrates as compared to undamaged DNA. Well-resolved XPA−DNA complexes were observed with the defined DNA substrate containing a γ-radiation-induced G[8,5-Me]T guanine−thymine cross-link lesion, and the complex formation was dependent on the concentrations of XPA. Since XPA binds to damaged DNA in a cooperative manner (*1*), XPA_2 dimer−DNA complexes formed at higher protein concentrations (Figure 1A, lanes 3−5) as determined previously (*1*). In contrast, RPA showed little affinity for the G[8,5-Me]T-containing substrate at protein concentrations ranging from 25 to 200 nM (Figure 1A, lanes 6−9), whereas RPA did interact with XPA-bound G[8,5-Me]T substrate to form a slower migrating band (Figure 1A, lanes 10−12). Evidently, the XPA protein efficiently recognized the G[8,5-Me]T lesion. By contrast, there was no detectable binding of XPA to the undamaged DNA duplex (dsDNA) or single-stranded DNA (ssDNA) even at 600 nM concentration of the protein (Figure 1B).

XPA Binding to Mismatched Nucleotide Bubble DNA Substrates. EMSA analysis of XPA interaction with six-nucleotide mismatched DNA substrates revealed that XPA had a high affinity for the DNA bubble structure with or without DNA damage (Figure 2A). For comparison, we examined the XPA interactions with DNA substrates containing an AF, AAF, AP, or T[6,4]T lesion in the six-nucleotide bubble structure (*34*). No significant difference in XPA binding was observed among these adducts. In addition, there was no difference in XPA binding between damaged or undamaged (ND) bubble substrates (Figure 2A). Binding of XPA to the bubble substrates was observed at protein concentrations as low as 2.5 nM (Figure 2A, lanes 2, 6, 10, 14, 18); such a high affinity of XPA−DNA (damaged or undamaged) interaction has not been previously reported. The effects of the DNA bubble size on the affinity of XPA also were investigated. Our results indicated that XPA recognized bubble structures with the size of four mismatched nucleotides or larger (Figure 2B, lanes 6−24). The protein appeared to have a higher affinity for the DNA substrate with an eight-base bubble or larger. XPA, however, did not efficiently recognize bubble structures smaller than four mismatched nucleotides (Figure 2B, lanes 1−4). A possible explanation we considered for this observation is that XPA recognizes ds-ssDNA junctions.

XPA Binds DNA Substrates with a 3′- or 5′-Overhang and Stabilizes RPA−DNA Interaction. We next investigated the affinity of XPA for 3′-overhang and 5′-overhang DNA substrates, two types of ds-ssDNA junctions. Weak binding was observed for each substrate at XPA protein concentrations lower than 50 nM (Figure 3A, lanes 3 and 9). However, at 100 nM concentration quantitative binding of the substrates with XPA was noted (Figure 3A, lanes 5 and 11), and no detectable difference in binding affinity was observed between the two substrates. RPA also interacted with the substrates due to its high affinity for the ssDNA regions (Figure 3B, lanes 2, 3, 8, and 9). Addition of XPA at a concentration of 10 nM appeared to enhance the binding of RPA for both overhang substrates (Figure 3B, lanes 5, 6, 11, and 12). As XPA itself exhibited only weak binding affinity for each of the substrates at this concentration, the enhancement was likely due to the stabilization of the RPA−DNA complex through XPA−RPA interactions. However, the contribution from the combined but separate bindings of XPA to the junction and RPA to the ssDNA region also cannot be ruled out. To further confirm that the band shift was due to the XPA−DNA complex formation, monoclonal anti-XPA antibody (Kamiya) was added to the reaction after incubation of XPA with the 5′-overhang DNA substrate. As shown in Figure 3C (lanes 4 and 5), the protein−DNA complex band was supershifted by the antibody, indicating that the protein binding to the DNA substrate indeed was XPA. As controls, antibody against the RPA32 subunit of RPA (Kamiya) also caused a supershift for the RPA−DNA complex (lanes 2 and 3), and there was no cross-interaction of anti-XPA antibody with this complex (lane 6) and vice versa (lane 7).

XPA Interaction with ds-ssDNA Junctions Containing both 3′- and 5′-ssDNA Overhangs (Y-Shape Structures). In order to examine the binding of XPA to the ds-ssDNA junction structure formed as intermediates in NER, we constructed a Y-shape ds-ssDNA junction substrate (Figure 4). EMSA analysis revealed that XPA efficiently bound to the Y-shape substrate (Figure 4A). Further determination by fluorescence anisotropy indicated that the binding had a K_d of 49.1 ± 5.1 nM (Figure 4B). Evidently, this binding affinity of XPA for Y-shape DNA is much higher than for damaged DNA (without bubble) that has a K_d of hundreds of nanomolar. Indeed, as shown in Figure 4C, although RPA had a higher affinity for the two ssDNA regions in the Y-shape substrate

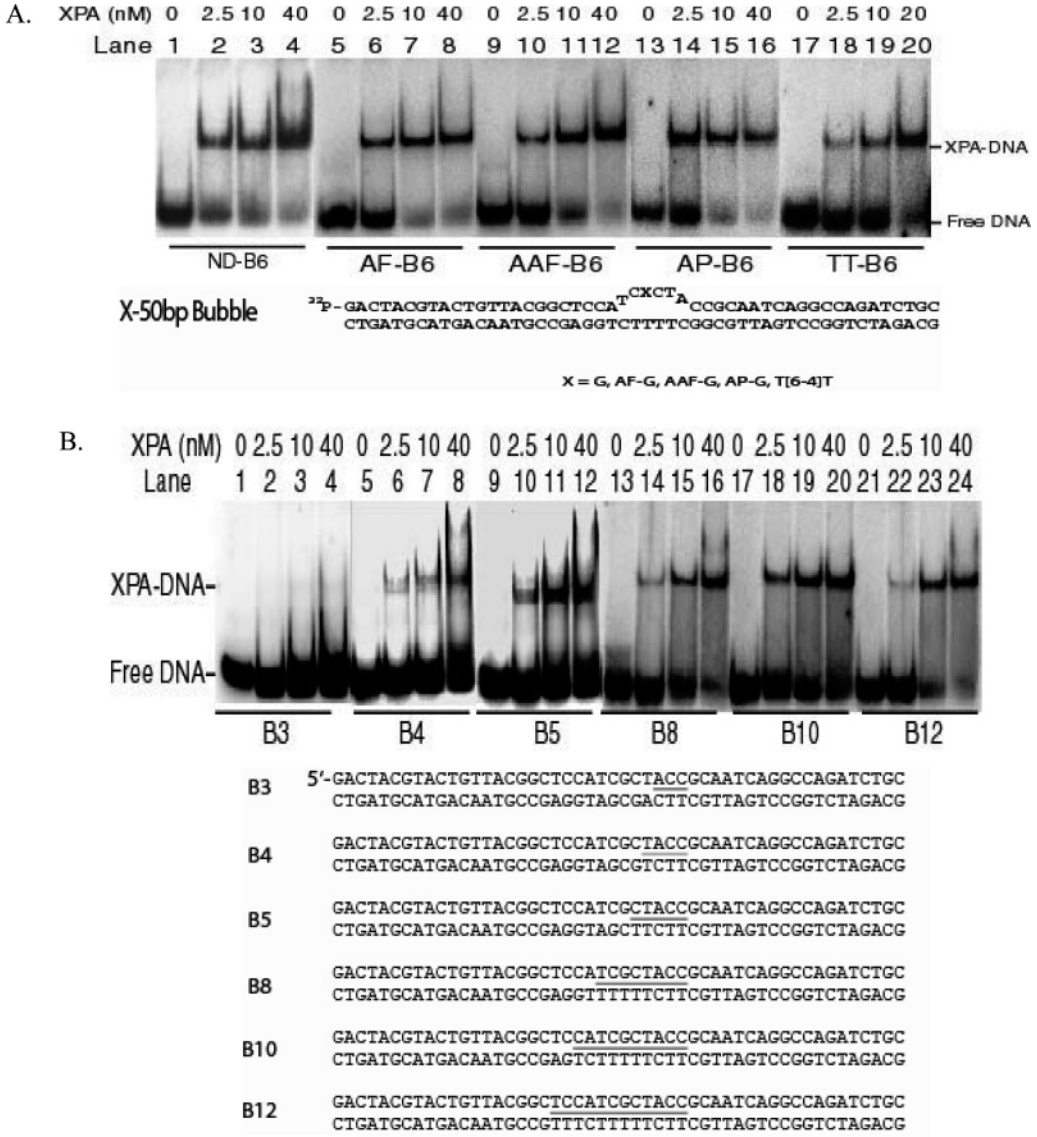

FIGURE 2: Binding of XPA protein to partially mismatched DNA bubble substrates with or without a lesion. Panel A: XPA bound to six-base mismatched DNA bubble substrates with or without AF, AAF, AP, or T[6,4]T adduct at varying concentrations. ND-B6 stands for undamaged DNA substrate containing a six-base mismatched bubble. Panel B: XPA bound to DNA substrates with various sizes of bubble. The underline in the sequences indicates the mismatched bases for bubble formation.

than XPA for the single junction (Figure 4C, lanes 2−5), XPA efficiently bound to the ds-ssDNA junction of the same substrate at a concentration as low as 10 nM (Figure 4C, lanes 10 and 11). It should be noted that the XPA had little affinity for dsDNA (Figure 1A) or ssDNA (data not shown). Interestingly, XPA appeared to slightly prefer binding to the ds-ssDNA junction of the Y-shape DNA molecules that were already bound by RPA (Figure 4C, lane 10), although there was a large excess of free DNA available for binding.

To confirm the direct contact of XPA with the ds-ssDNA junction with ssDNA overhangs and to define the size of the binding, we mapped the binding sites of XPA to the DNA substrate using both DNase I and permanganate ($KMnO_4$) footprinting assays. DNase I is best for dsDNA footprinting as it has a much higher nuclease activity toward dsDNA than ssDNA (*33*). In contrast, $KMnO_4$ selectively attacks thymines in ssDNA. As shown in Figure 5, the Y-shape ds-ssDNA junction substrate contains a string of thymines in the ssDNA region of the bottom strand. Thus, the substrate was radiolabeled with ^{32}P at the 5′-end of the bottom strand for use in the footprinting assays. As shown in Figure 5, binding of XPA to the substrate resulted in a significant protection from DNase I of the dsDNA region of about 7 nucleotides 3′ (labeled bottom strand) to the junction (lanes 1 and 2), while about 12 nucleotides were shielded from $KMnO_4$ oxidation in the ssDNA region 5′ to the junction (lanes 4 and 5). Lane 3 showed the DNase I digestion of a double-stranded 50 bp DNA for control. The footprinting results indicated that the XPA did bind to the ds-ssDNA junction.

Since XPA binds to damaged DNA as a protein homodimer as described previously (*1*), next we asked the question of whether XPA binds to the ds-ssDNA junction in the same or different oligomeric forms. The above results of gel mobility shift assays in which the XPA−DNA junction complex migrated much faster than the XPA dimer-damaged DNA complex (the second band shift in Figure 1) (*1*) suggest that XPA may interact with the ds-ssDNA junction as a monomer. This was further supported by a gel filtration assay combined with the liquid scintillation counting for determination of the stoichiometry of XPA−Y-shape DNA substrate

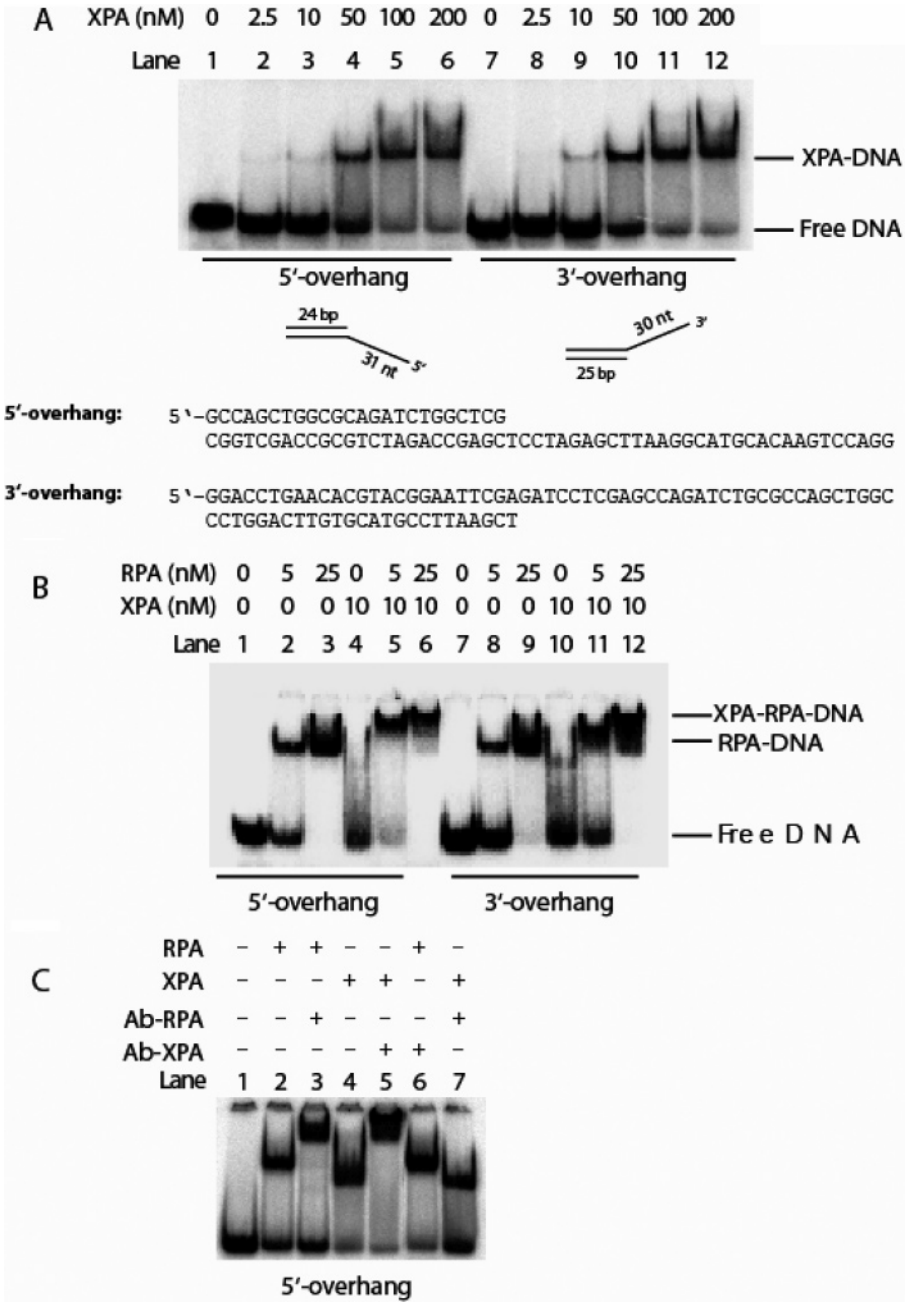

FIGURE 3: Interactions of XPA and/or RPA with 3′- and 5′-single-strand overhang DNA substrates. Panel A: XPA bound to 3′-ssDNA overhang and 5′-ssDNA overhang DNA substrates at various concentrations. Panel B: XPA and RPA interacted with the 3′-overhang and 5′-overhang DNA substrates. Panel C: XPA and RPA interacted with the 5′-overhang DNA substrate, and the complexes were supershifted with corresponding antibodies, respectively.

binding. As shown in Figure 6, a retention volume of 13.2 mL was obtained for the XPA−Y-shape DNA complex when eluted from a Superdex 200 column. In contrast, the XPA dimer−damaged DNA complex was eluted earlier at 12.2 mL (Figure 6) (*1*), while free DNA was eluted much later at a retention volume of about 22 mL (Figure 6). The corresponding apparent molecular mass of the complex was calculated to be ~70 kDa based on a standard plot of retention volumes versus the log of the molecular weights of standard protein markers (*1*). This suggested that the molecular ratio of protein to DNA is 1:1 (XPA MW, 36 kDa; Y-shape DNA MW, 33.7 kDa) (Figure 6). It should be noted, however, that this determination was based on the assumption that the protein−DNA complex primarily has a globular structure with the bound DNA as part of it, whereas the free DNA was eluted anomalously due to its linear structure. Nonetheless, the fact that the XPA−Y-shape DNA complex has a larger retention volume than the complex of XPA dimer with damaged DNA supports a monomeric form of XPA binding to the ds-ssDNA junction. The same results were also obtained for XPA interaction with the 3′-overhang DNA (data not shown). As compared with the dimeric form of XPA needed for DNA damage recognition, these results support a new function for the protein. The XPA interaction with ds-ssDNA junctions was further supported by our in vivo evidence in which significant amounts of immunofluorescent XPA nuclear foci formed in human diploid fibroblasts BJ cells with the PCNA knock down by siRNA (submitted for publication). By contrast, no XPA nuclear foci formed in the same cells transfected with GFP siRNA. PCNA is an

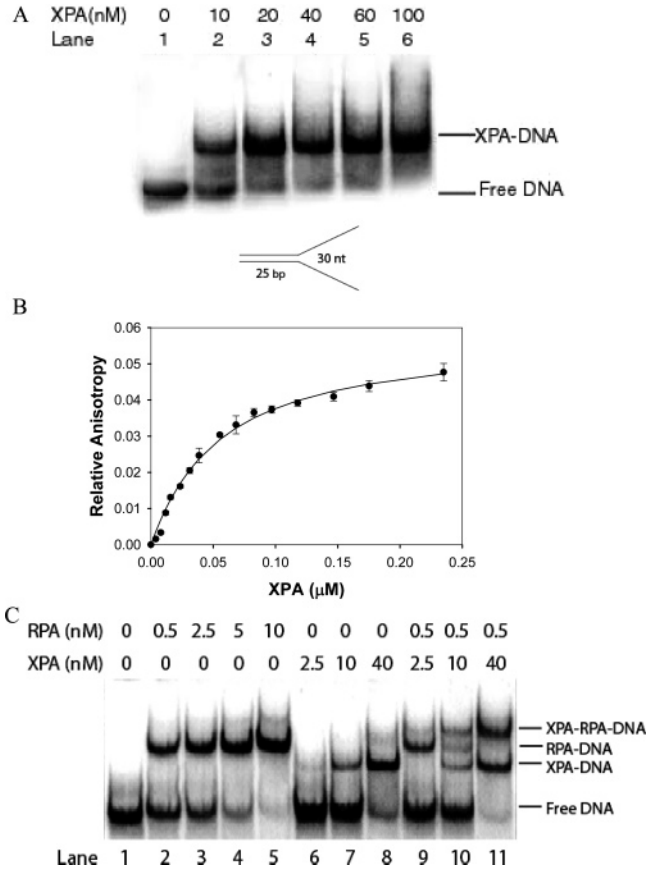

FIGURE 4: Binding of XPA to Y-shape DNA substrate in the presence and absence of RPA. Panel A: XPA bound to the Y-shape DNA substrate in an XPA concentration-dependent manner. Panel B: Fluorescence anisotropy measurements of XPA binding to the ds-ssDNA junction substrate. The binding isotherms were generated by titrating the substrate with increasing concentrations of XPA. Panel C: XPA and/or RPA bound to Y-shape DNA. RPA bound to the single-strand regions of the Y-shape substrate (lanes 2−5), while XPA bound to the ds-ssDNA junction of the substrate (lanes 6−8). When both XPA and RPA were present, formation of three complexes was observed corresponding to XPA binding to the ds-ssDNA junction (XPA−DNA), RPA binding to the ssDNA regions of the substrate (RPA−DNA), and XPA and RPA concurrently binding to the junction and ssDNA regions of the same substrate molecules (XPA−RPA−DNA), respectively (lanes 10 and 11).

essential factor required for protein binding of ds-ssDNA junction intermediates at replication forks and many other DNA metabolic processes.

XPC−HR23B, not XPA or XPA−RPA, Recognizes DNA Bending. Although XPC or XPC−HR23B was previously reported to recognize DNA bending structures (*35*), the XPA protein also has been proposed as a recognition factor for DNA bending (*16*). In order to determine which protein/complex might be responsible for recognition of DNA bending induced by DNA damage, and the DNA structural determinants recognized by XPA, we constructed a set of DNA substrates (50 bp) containing different degrees of DNA bending. These bendings were introduced through a simple two-, three-, or four-carbon tether cross-linking two adjacent guanines in the middle of the sequence (*30*) (Materials and Methods). The length of the tether in these substrates was indicated as 2-C, 3-C, 4-C, etc. The bending angles of the DNA substrates were determined to be 30° for 2-C, 11.7° for 3-C, and 7.4° for 4-C (*30*). Thus, EMSA was employed to examine the binding of homogeneous XPA and XPC−

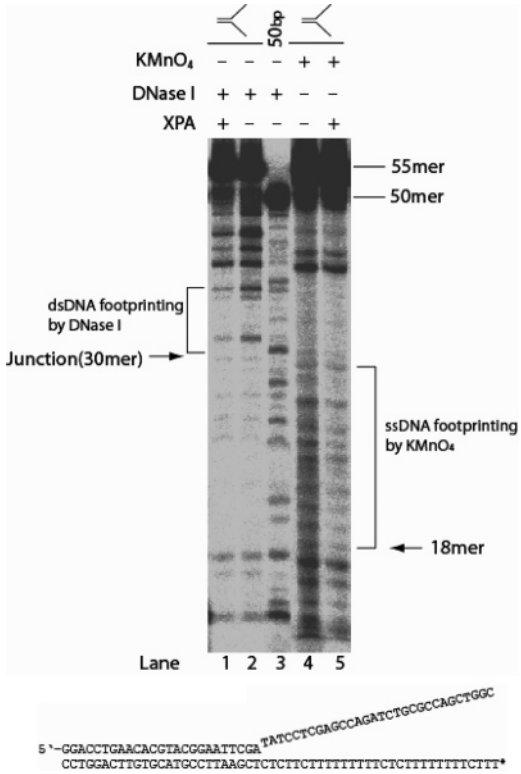

FIGURE 5: Footprinting of XPA binding to the ds-ssDNA junctions in the Y-shape substrate with 3′- and 5′-ssDNA overhangs. Lanes 1−3: dsDNA footprinting by DNase I. Lanes 4 and 5: ssDNA footprinting by $KMnO_4$. Y-shape substrates with a ^{32}P-labeled 5′-end of the bottom strand (indicated by the asterisk) were incubated at 30 °C for 15 min in binding buffer with or without XPA. After the incubation, substrates were digested with 0.7 ng of DNase I (lanes 1−3) or probed with 0.2 mM $KMnO_4$ (lanes 5 and 6), followed by hot piperidine treatment. Both footprinting reactions were performed at room temperature for 1 min. The samples were analyzed on a 12% denaturing polyacrylamide gel.

HR23B to each of the bent DNA substrates. Neither XPA (Figure 7A) nor XPA−RPA (data not shown) showed any detectable affinity for these bent DNAs. By clear contrast, XPC−HR23B efficiently recognized DNA bending with the affinity in the following order, 2-C > 3-C > 4-C > 0-C (i.e., no tether) (Figure 7B), which correlated with the degrees of bending angle of these substrates. To further confirm the results, the same substrates were subjected to binding with UvrA, the *E. coli* NER DNA damage recognition protein, which has been known to recognize DNA bending. As shown in Figure 7C, UvrA did bind to the substrates with the affinity increasing with bending angles. These results strongly suggest that the XPC−HR23B complex, rather than XPA, is the factor that recognizes DNA bending, further supporting the XPA recognition of other types of DNA structures such as ds-ssDNA junctions.

DISCUSSION

DNA damage recognition in human NER utilizes cooperative binding and kinetic proofreading to provide a physiologically relevant mechanism by which DNA damage is efficiently discriminated and identified from a vast excess of undamaged DNA (*4*, *36*). In comparison with XPC−HR23B, XPA appears to play a supporting role in DNA damage recognition. This appears to be inconsistent with the physiological significance of XPA in NER as XPA-deficient

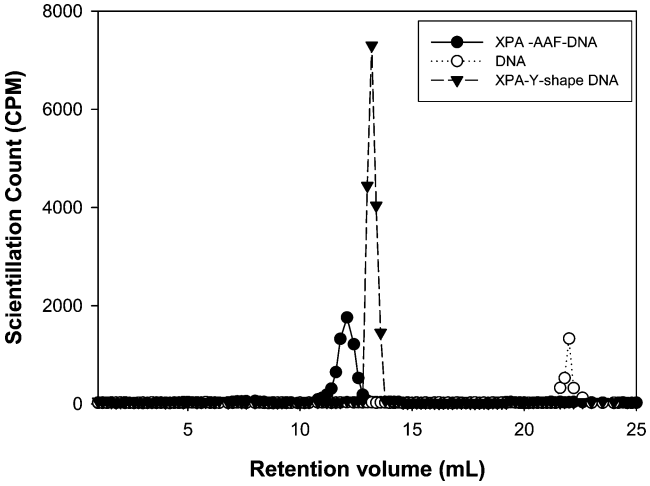

FIGURE 6: Gel filtration−scintillation analysis for determination of the stoichiometry of XPA binding to Y-shape DNA. XPA of 40 and 1000 nM was incubated with radiolabeled Y-shape and AAF−50 bp DNA substrates, respectively, and analyzed by gel filtration chromatography on a Superdex 200 column. The eluted fractions were then subjected to scintillation counting. Radioactivity profiles of the XPA−DNA complexes versus retention volume show that the XPA−Y-shape DNA complex was eluted at 13.2 mL (▼), as compared to XPA−AAF−DNA complex at 12.2 mL (●) (*1*). Free DNA was eluted at ∼22 mL (○). Determination of apparent molecular weights of the XPA−DNA complexes based on a linear relationship between the molecular weights of protein markers and their retention times suggests that XPA may bind to the Y-shape DNA substrate as a monomer.

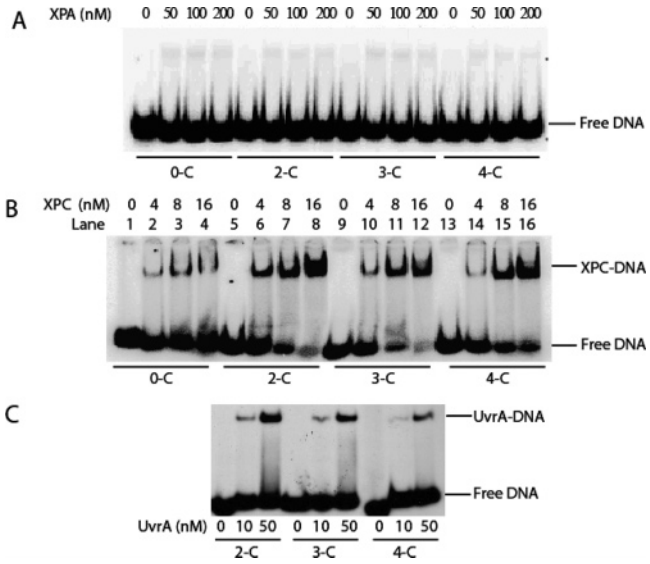

FIGURE 7: Recognition of DNA bending by XPA or the XPC−HR23B complex. Panel A: XPA displayed no significant affinity for any of the substrates with DNA bending induced by a two-carbon (2-C), three-carbon (3-C), or four-carbon (4-C) tether cross-linking two adjacent guanines. The 0-C stands for unmodified DNA with no bending (no carbon tether). Panel B: The XPC−HR23B complex (labeled as XPC) had high affinities to DNA bending with the following order, 2-C > 3-C > 4-C > 0-C, which is consistent with the order of their bending angles, 2-C > 3-C > 4-C > 0-C. Panel C: Binding of *E. coli* UvrA to the same DNA bending substrates (*27*−*29*).

cells are extremely sensitive to UV and also much more sensitive than the cells deficient in XPC, the major damage recognition protein in NER. Although the functions of XPA in NER have been extensively studied, the details of its role, particularly in TCR where XPC−HR23B is not required, remain unclear. All of these imply that XPA may have other additional functions in NER. In the present study, we report that, in addition to its involvement in DNA damage recognition, XPA demonstrated a novel biochemical activity in binding the biologically important DNA structures: the undamaged ds-ssDNA junctions with ssDNA branches, including the ssDNA-branched Y-structure junction and the junctions with either a 3′- or 5′-ssDNA overhang. While XPA was previously shown to be able to efficiently bind double-stranded three-way or four-way (Holliday junction-type) DNA structures, no affinity of XPA for the Y-shape ds-ssDNA junctions with ssDNA overhangs was observed (*16*, *17*). The discrepancy is likely due to the use of different experimental conditions for the protein−DNA binding and the XPA proteins purified from different systems. In the present study, the human XPA was expressed in and purified to homogeneity from insect cells instead of *E. coli*. In addition, the three- and four-way dsDNA structures were used to mimic the helical kinks induced by DNA damage which were believed to be recognized by XPA, although no such structures formed as intermediates during NER (*16*, *17*). By contrast, the undamaged ds-ssDNA junctions with ssDNA branches are the intermediate DNA structures formed during NER.

The binding of XPA to the ds-ssDNA junction may mimic its interaction with the ds-ssDNA junctions formed during NER. Following initial DNA damage recognition, an opened DNA structure of ∼25 nt around the lesion forms with TFIIH as a crucial intermediate in NER (*37*). In TCR, such DNA strand opening is present through the entire process of transcription. It is clear that the ds-ssDNA junction is a major structural characteristic of the intermediate. Therefore, we wished to determine how the size of the DNA opening is defined and how an opened DNA structure is stabilized in NER. We were also interested in elucidating how the nucleases are recruited to the right sites for incisions and the role of XPA in TCR where RNA polymerase complex is believed to carry out the initial DNA damage recognition. Our finding of XPA binding to ds-ssDNA junctions shed some light on these issues. The ability of XPA to recognize the ds-ssDNA junctions with such a high affinity suggests that the XPA−DNA junction binding may play a role in stabilizing the DNA opening following DNA unwinding at the lesion site by TFIIH. XPA may also stabilize the TFIIH−DNA interaction and, thus, define the size of the strand opening. This is supported by the previous reports that the recruitment of the TFIIH complex to the repair site was promoted by the presence of XPA (*19*, *21*). On the other hand, XPA has been suggested to play a direct role in recruiting the ERCC1-XPF nuclease to the repair complex for 5′-incision of damaged DNA (*18*, *22*) at the sites near the ds-ssDNA junction (*37*). It has been suggested that this recruitment was carried out by the XPA binding to the DNA lesion. The much higher affinity of XPA for the junctions relative to the DNA damage raises the question if DNA junction binding might be the major function of XPA in NER. This activity also provides an explanation for XPA's role in both GGR and TCR and the observation that XPA remains on the repair complex through the late stage of NER (*12*, *38*).

Different from the dimeric form of XPA in DNA damage recognition, this XPA−ds-ssDNA junction binding activity

appears to be exclusively delivered by the XPA monomer, supporting that XPA may have at least two different DNA recognition activities: one is for damaged DNA while the other is for undamaged DNA. Interestingly, ds-ssDNA junctions are a common DNA intermediate structure formed in many DNA metabolic processes including DNA repair, replication, and recombination, implying a potential additional role of XPA in cellular processes. In support, a recent report indicated that ATR checkpoint signaling is compromised in UV-irradiated XPA-deficient human cells during the S-phase (*39*). Since activation of the ATR checkpoint is replication dependent and a large number of ds-ssDNA junction intermediates form at replication forks, our finding provides some insights into the possible mechanism of the ATR signaling−XPA relationship.

It is well established that XPA can form complexes with RPA. Since RPA is a ssDNA binding protein, the ssDNA regions next to a ds-ssDNA junction offer a biological platform for RPA to interact with XPA bound to the junction. Such protein−protein interaction may help to stabilize, in a cooperative manner, the opened DNA structure of the repair complex and intermediates necessary for DNA damage incisions.

With respect to the role of XPA in DNA damage recognition as compared with that of the XPC−HR23B complex, we also examined the interaction of these proteins with bent DNA, which is often induced by bulky DNA lesions. We synthesized a set of defined DNA bending substrates with defined bending angles. Our results indicated that XPA had little affinity toward DNA bending up to 30°. By contrast, the XPC−HR23B complex efficiently recognized this DNA distortion. This is consistent with the role of XPC−HR23B in the initial DNA damage recognition in GGR. The results also are consistent with the fact that in TCR which requires XPA but not XPC−HR23B, no DNA bending could form at the lesion due to its location within a large DNA strand opening. Despite these, our results could not rule out the possibility of XPA binding to DNA bending with greater bending angles, such as those induced by cisplatin-GG intrastrand cross-link (50−60°) (*40*) and by (*6-4*) photoproducts (44°) (*41*). Nevertheless, these lesions concurrently introduce a large degree of DNA unwinding and twist, some of the major DNA helical distortions that are also induced by several DNA monoadducts and recognized by DNA repair proteins. Taken together, our results indicate that the XPC−HR23B complex has a much higher preference over XPA for recognition of DNA bending.

ACKNOWLEDGMENT

We thank Drs. Douglas P. Thewke and David Johnson for technical help on the initial propagation of the recombinant viruses and for optimizing protein−DNA interaction conditions.

REFERENCES

1. Liu, Y., Liu, Y., Yang, Z., Utzat, C., Wang, G., Basu, A. K., and Zou, Y. (2005) Cooperative interaction of human XPA stabilizes and enhances specific binding of XPA to DNA damage, *Biochemistry 44*, 7361−7368.
2. Wood, R. D. (1999) DNA damage recognition during nucleotide excision repair in mammalian cells, *Biochimie 81*, 39−44.
3. Thoma, B. S., and Vasquez, K. M. (2003) Critical DNA damage recognition functions of XPC-hHR23B and XPA-RPA in nucleotide excision repair, *Mol. Carcinog. 38*, 1−13.
4. Sancar, A., Lindsey-Boltz, L. A., Unsal-Kacmaz, K., and Linn, S. (2004) Molecular mechanisms of mammalian DNA repair and the DNA damage checkpoints, *Annu. Rev. Biochem. 73*, 39−85.
5. Reardon, J. T., and Sancar, A. (2005) Nucleotide excision repair, *Prog. Nucleic Acid Res. Mol. Biol. 79*, 183−235.
6. Yang, Z. G., Liu, Y., Mao, L. Y., Zhang, J. T., and Zou, Y. (2002) Dimerization of human XPA and formation of XPA2-RPA protein complex, *Biochemistry 41*, 13012−13020.
7. Sugasawa, K., Ng, J. M., Masutani, C., Iwai, S., van der Spek, P. J., Eker, A. P., Hanaoka, F., Bootsma, D., and Hoeijmakers, J. H. (1998) Xeroderma pigmentosum group C protein complex is the initiator of global genome nucleotide excision repair, *Mol. Cell 2*, 223−232.
8. Wang, M., Mahrenholz, A., and Lee, S. H. (2000) RPA stabilizes the XPA-damaged DNA complex through protein-protein interaction, *Biochemistry 39*, 6433−6439.
9. Hermanson-Miller, I. L., and Turchi, J. J. (2002) Strand-specific binding of RPA and XPA to damaged duplex DNA, *Biochemistry 41*, 2402−2408.
10. Patrick, S. M., and Turchi, J. J. (2002) Xeroderma pigmentosum complementation group A protein (XPA) modulates RPA-DNA interactions via enhanced complex stability and inhibition of strand separation activity, *J. Biol. Chem. 277*, 16096−16101.
11. Rademakers, S., Volker, M., Hoogstraten, D., Nigg, A. L., Mone, M. J., Van Zeeland, A. A., Hoeijmakers, J. H., Houtsmuller, A. B., and Vermeulen, W. (2003) Xeroderma pigmentosum group A protein loads as a separate factor onto DNA lesions, *Mol. Cell. Biol. 23*, 5755−5767.
12. Riedl, T., Hanaoka, F., and Egly, J. M. (2003) The comings and goings of nucleotide excision repair factors on damaged DNA, *EMBO J. 22*, 5293−5303.
13. Hey, T., Lipps, G., and Krauss, G. (2001) Binding of XPA and RPA to damaged DNA investigated by fluorescence anisotropy, *Biochemistry 40*, 2901−2910.
14. Thoma, B. S., Wakasugi, M., Christensen, J., Reddy, M. C., and Vasquez, K. M. (2005) Human XPC-hHR23B interacts with XPA-RPA in the recognition of triplex-directed psoralen DNA interstrand crosslinks, *Nucleic Acids Res. 33*, 2993−3001.
15. Koberle, B., Roginskaya, V., and Wood, R. D. (2006) XPA protein as a limiting factor for nucleotide excision repair and UV sensitivity in human cells, *DNA Repair (Amsterdam) 5*, 641−648.
16. Missura, M., Buterin, T., Hindges, R., Hubscher, U., Kasparkova, J., Brabec, V., and Naegeli, H. (2001) Double-check probing of DNA bending and unwinding by XPA-RPA: an architectural function in DNA repair, *EMBO J. 20*, 3554−3564.
17. Camenisch, U., Dip, R., Schumacher, S. B., Schuler, B., and Naegeli, H. (2006) Recognition of helical kinks by xeroderma pigmentosum group A protein triggers DNA excision repair, *Nat. Struct. Mol. Biol.* (in press).
18. Park, C. H., and Sancar, A. (1994) Formation of a ternary complex by human XPA, ERCC1, and ERCC4(XPF) excision repair proteins, *Proc. Natl. Acad. Sci. U.S.A. 91*, 5017−5021.
19. Park, C. H., Mu, D., Reardon, J. T., and Sancar, A. (1995) The general transcription-repair factor TFIIH is recruited to the excision repair complex by the XPA protein independent of the TFIIE transcription factor, *J. Biol. Chem. 270*, 4896−4902.
20. Guzder, S. N., Sung, P., Prakash, L., and Prakash, S. (1996) Nucleotide excision repair in yeast is mediated by sequential assembly of repair factors and not by a pre-assembled repairosome, *J. Biol. Chem. 271*, 8903−8910.
21. Nocentini, S., Coin, F., Saijo, M., Tanaka, K., and Egly, J. M. (1997) DNA damage recognition by XPA protein promotes efficient recruitment of transcription factor II H, *J. Biol. Chem. 272*, 22991−22994.
22. Guzder, S. N., Sommers, C. H., Prakash, L., and Prakash, S. (2006) Complex formation with damage recognition protein Rad14 is essential for *Saccharomyces cerevisiae* Rad1-Rad10 nuclease to perform its function in nucleotide excision repair in vivo, *Mol. Cell. Biol. 26*, 1135−1141.
23. Liu, Y., Yang, Z., Utzat, C. D., Liu, Y., Geacintov, N. E., Basu, A. K., and Zou, Y. (2005) Interactions of human replication protein A with single-stranded DNA adducts, *Biochem. J. 385*, 519−526.
24. Reardon, J. T., Mu, D., and Sancar, A. (1996) Overproduction, purification, and characterization of the XPC subunit of the human DNA repair excision nuclease, *J. Biol. Chem. 271*, 19451−19456.

25. Manley, J. L., Fire, A., Cano, A., Sharp, P. A., and Gefter, M. L. (1980) DNA-dependent transcription of adenovirus genes in a soluble whole-cell extract, *Proc. Natl. Acad. Sci. U.S.A. 77*, 3855−3859.
26. Manley, J. L., Fire, A., Samuels, M., and Sharp, P. A. (1983) In vitro transcription: whole-cell extract, *Methods Enzymol. 101*, 568−582.
27. Zou, Y., Luo, C., and Geacintov, N. E. (2001) Hierarchy of DNA damage recognition in *Escherichia coli* nucleotide excision repair, *Biochemistry 40*, 2923−2931.
28. Zou, Y., Shell, S. M., Utzat, C. D., Luo, C., Yang, Z., Geacintov, N. E., and Basu, A. K. (2003) Effects of DNA adduct structure and sequence context on strand opening of repair intermediates and incision by UvrABC nuclease, *Biochemistry 42*, 12654−12661.
29. Yang, Z., Colis, L. C., Basu, A. K., and Zou, Y. (2005) Recognition and incision of gamma-radiation-induced cross-linked guanine-thymine tandem lesion G[8, 5-Me]T by UvrABC nuclease, *Chem. Res. Toxicol. 18*, 1339−1346.
30. Kowalczyk, A., Carmical, J. R., Zou, Y., Van Houten, B., Lloyd, R. S., Harris, C. M., and Harris, T. M. (2002) Intrastrand DNA cross-links as tools for studying DNA replication and repair: two-, three-, and four-carbon tethers between the N(2) positions of adjacent guanines, *Biochemistry 41*, 3109−3118.
31. Liu, Y., Kvaratskhelia, M., Hess, S., Qu, Y., and Zou, Y. (2005) Modulation of replication protein A function by its hyperphosphorylation-induced conformational change involving DNA binding domain B, *J. Biol. Chem. 280*, 32775−32783.
32. Zou, Y., Liu, T. M., Geacintov, N. E., and Van Houten, B. (1995) Interaction of the UvrABC nuclease system with a DNA duplex containing a single stereoisomer of dG-(+)- or dG-(−)-anti-BPDE, *Biochemistry 34*, 13582−13593.
33. Zou, Y., and Van Houten, B. (1999) Strand opening by the UvrA(2)B complex allows dynamic recognition of DNA damage, *EMBO J. 18*, 4889−4901.
34. Luo, C., Krishnasamy, R., Basu, A. K., and Zou, Y. (2000) Recognition and incision of site-specifically modified C8 guanine adducts formed by 2-aminofluorene, *N*-acetyl-2-aminofluorene and 1-nitropyrene by UvrABC nuclease, *Nucleic Acids Res. 28*, 3719−3724.
35. Janicijevic, A., Sugasawa, K., Shimizu, Y., Hanaoka, F., Wijgers, N., Djurica, M., Hoeijmakers, J. H., and Wyman, C. (2003) DNA bending by the human damage recognition complex XPC-HR23B, *DNA Repair (Amsterdam) 2*, 325−336.
36. Reardon, J. T., and Sancar, A. (2004) Thermodynamic cooperativity and kinetic proofreading in DNA damage recognition and repair, *Cell Cycle 3*, 141−144.
37. Evans, E., Moggs, J. G., Hwang, J. R., Egly, J. M., and Wood, R. D. (1997) Mechanism of open complex and dual incision formation by human nucleotide excision repair factors, *EMBO J. 16*, 6559−6573.
38. Tapias, A., Auriol, J., Forget, D., Enzlin, J. H., Scharer, O. D., Coin, F., Coulombe, B., and Egly, J. M. (2004) Ordered conformational changes in damaged DNA induced by nucleotide excision repair factors, *J. Biol. Chem. 279*, 19074−19083.
39. Bomgarden, R. D., Lupardus, P. J., Soni, D. V., Yee, M. C., Ford, J. M., and Cimprich, K. A. (2006) Opposing effects of the UV lesion repair protein XPA and UV bypass polymerase eta on ATR checkpoint signaling, *EMBO J. 25*, 2605−2614.
40. Kozelka, J., Petsko, G. A., Quigley, G. J., and Lippard, S. J. (1986) High-salt and low-salt models for kinked adducts of cis-diamminedichloroplatinum(II) with oligonucleotide duplexes, *Inorg. Chem. 25*, 1075−1077.
41. Kim, J. K., Patel, D., and Choi, B. S. (1995) Contrasting structural impacts induced by cis-syn cyclobutane dimer and (6-4) adduct in DNA duplex decamers: implication in mutagenesis and repair activity, *Photochem. Photobiol. 62*, 44−50.
42. Wu, X., Shell, S. M., Liu, Y., and Zou, Y. (2006) ATR-dependent checkpoint modulates XPA nuclear import in response to UV irradiation, *Oncogene* (Jul 24; Epub ahead of print).
43. Wu, X., Shell, S. M., Yang, Z., and Zou, Y. (2006) Phosphorylation of nucleotide excision repair factor xeroderma pigmentosum group A by ataxia telangiectasia mutated and Rad3-related-dependent checkpoint pathway promotes cell survival in response to UV irradiation, *Cancer Res. 66*, 2997−3005.

BI061626Q